iScience

CellPress
OPEN ACCESS

Article

Redox manipulation of enzyme activity through physiologically active molecule

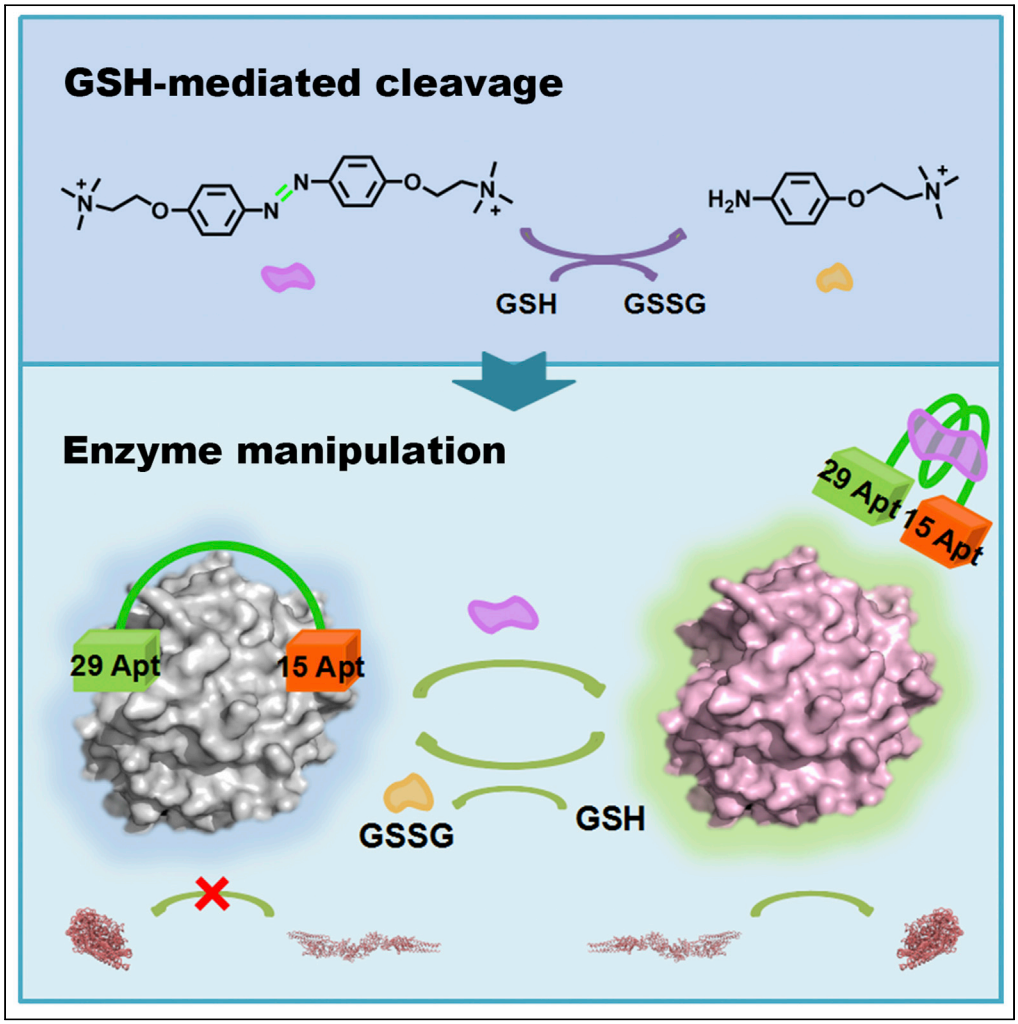

Dao Lin, Yuhe Kan, Liang Yan, ..., Xiangjun Li, Yujian He, Li Wu

wuli@ucas.ac.cn (L.W.)
lixiangj@ucas.ac.cn (X.L.)
heyujian@ucas.ac.cn (Y.H.)

Highlights

The transition of telomere DNA structures based on redox switch

Achieving redox manipulation of thrombin activity through active substance

This switch can be specifically used for enzyme regulation in cancer cells

Lin et al., iScience 24, 102977
September 24, 2021
https://doi.org/10.1016/j.isci.2021.102977

iScience

CellPress
OPEN ACCESS

Article

Redox manipulation of enzyme activity through physiologically active molecule

Dao Lin,[1] Yuhe Kan,[1] Liang Yan,[1] Yongqi Ke,[1] Yang Zhang,[1] Hang Luo,[1] Xinjing Tang,[2] Xiangjun Li,[1,*] Yujian He,[1,*] and Li Wu[1,2,3,*]

SUMMARY

The effective utility of physiologically active molecules is crucial in numerous biological processes. However, the regulation of enzyme functions through active substances remains challenging at present. Here, glutathione (GSH), produced in cells, was used to modulate the catalytic activity of thrombin without external stimulus. It was found that high concentrations of GSH was more conducive to initiate the cleavage of compound AzoDiTAB in the range of concentration used to mimic the difference between cancer and normal cells, which has practical implications for targeting cancel cells since GSH is overexpressed in cancer cells. Importantly, GSH treatment caused the deformation of G4 structure by cleaving AzoDiTAB and thus triggered the transition of thrombin from being free to be inhibited in complex biological systems. This work would open up a new route for the specific manipulation of enzyme-catalyzed systems in cancer cells.

INTRODUCTION

Enzymes are essential for affecting tumor growth (Rane and Minden, 2019; Wu et al., 2018; Wang et al., 2013). Precise manipulation of enzyme activity helps to drive biological processes in a positive direction, thus the development of excellent regulation strategies has received widespread attention. In most cases, the functions of enzymes can be manipulated by physical and chemical stimulus. For example, light can change the binding affinity between light-sensitive domains, leading to conversion of the protein function and signaling pathway (Tischer and Weiner, 2014; Zhang and Cui, 2015; Guglielmi et al., 2016). Encapsulation or liberation of enzymes in DNA cages depends on the pH in surrounding environment (Kim et al., 2017). Interestingly, the redox process of small molecules achieves the release of specific substrates, such as peptides (Lee et al., 2014; Bauri et al., 2018) and therapeutic agents (Medina et al., 2013; Eom et al., 2018; Zhang et al., 2017), without external stimulus, and this redox process has been used in the inhibition of arginine phosphatase YwlE by inducing disulfide bond formation (Fuhrmann et al., 2013). In fact, there are a large number of physiologically active molecules in cancer cells that can undergo redox processes (Trachootham et al., 2009), which have great potential in the regulation of enzyme activity.

Glutathione (GSH), a physiological active molecule produced in cell, is a ubiquitous tripeptide (Kosower and Kosower, 1978). GSH is essential for the cellular metabolism of various enzymes, hormones, and amino acids (Meister 1994; Anderson 1998). Previous evidence has demonstrated intracellular GSH concentration is in the millimolar range (0.5–10 mM (Kosower and Kosower, 1978; Hwang et al., 1992). Strikingly, GSH concentration is much higher in cancer tissues such as breast (Raderer and Scheithauer, 1993; Perry et al., 1993), colon (Berger et al., 1994; Redmond et al., 1991), lung (Oberlischrammli et al., 1994; Cook et al., 1991), bone marrow (Joncourt et al., 1995), ovary (Raderer and Scheithauer, 1993), and larynx (Mulder et al., 1995) compared with normal tissue. Moreover, GSH can be transferred to the surface, acting at the interface between the extracellular space and the membrane (Saito et al., 2003). These features have exhibited potential application in development of anticancer drug delivery system. A crucial feature of GSH is its ability to initiate the reduction of S-S bond (Lee et al., 2013) and N=N double bond (Zhang et al., 2017; Boulegue et al., 2007; Samanta et al., 2013; Kosower and Kanetylondner, 1976). Azo compounds play a special role in biological application due to its cis-trans structure (Hull et al., 2018; Lubbe et al., 2017). Furthermore, it has been found that the response of azobenzene molecules to GSH is closely related to its substituents (Samanta et al., 2013; Kosower and Kanetylondner, 1976). N=N double bond with higher electron cloud density is more protonated and accompanied by an increase in electrophilicity, which enhances the attack of sulfur group of GSH (Samanta et al., 2013).

[1]School of Chemical Sciences, University of Chinese Academy of Sciences, Beijing 101408, China

[2]State Key Laboratory of Natural and Biomimetic Drugs, School of Pharmaceutical Sciences, Peking University, Beijing 100191, China

[3]Lead contact

*Correspondence: wuli@ucas.ac.cn (L.W.), lixiangj@ucas.ac.cn (X.L.), heyujian@ucas.ac.cn (Y.H.)

https://doi.org/10.1016/j.isci.2021.102977

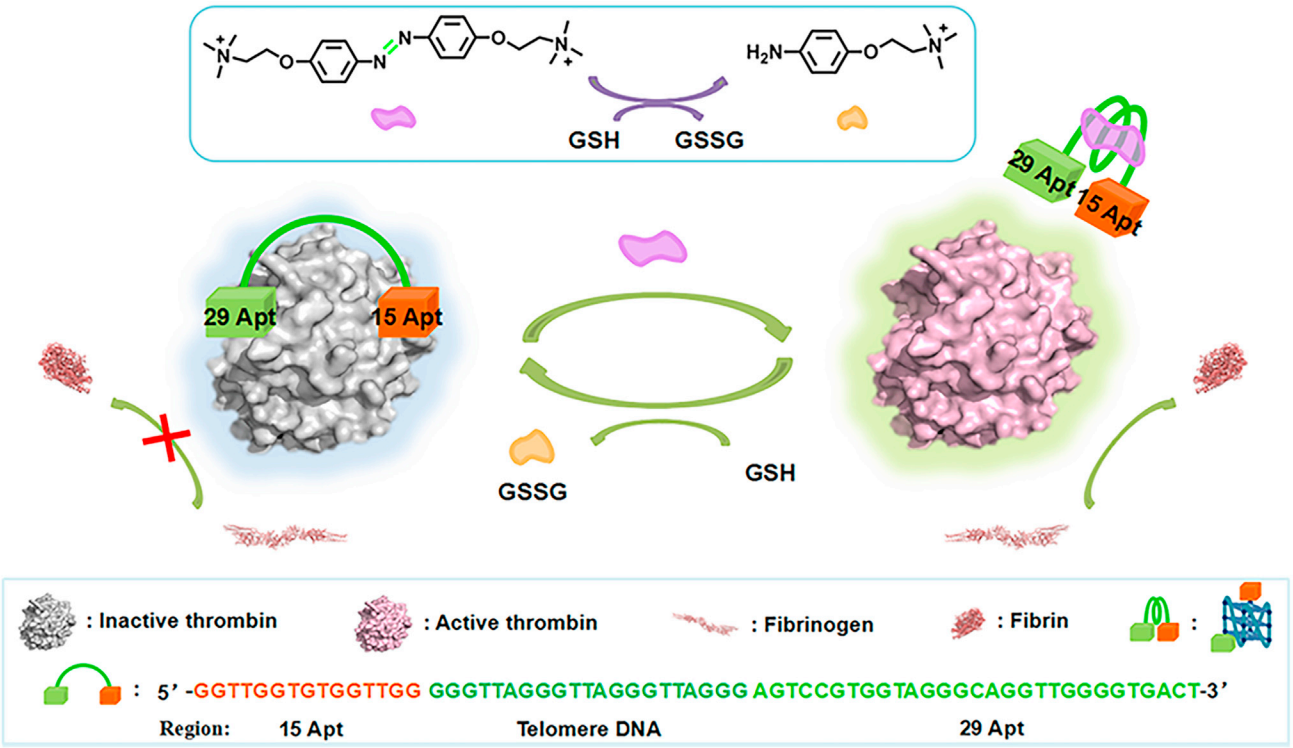

Scheme 1. Schematic representation of regulation of thrombin activity through active GSH

We intend to exploit a strategy to specifically regulate the enzyme function through GSH-mediated cleavage of azo compounds. An important step towards our goal is the acquisition of enzyme aptamers. It is reported that nucleic acid ligands with high affinity and recognition are a class of excellent enzyme aptamer (Panigaj et al., 2019). Remarkably, small molecules such as azobenzenes can be embedded in nucleic acid segments to optimize the DNA function (Mo et al., 2019; Haydell et al., 2018; Kim et al., 2009). G-quadruplex being a natural nucleic acid ligand has garnered intense interest due to its high-ordered molecular structure (Mergny and Sen, 2019; Biffi et al., 2013). Many approaches based on modification of the oligonucleotide itself to improve stability or performance have been explored (Kovacic et al., 2020; Virgilio et al., 2015; Pasternak et al., 2011). Moreover, researchers have designed some small molecules to control G4 structure through surface proximity hybridization. Among them, the photosensitive azobenzene derivative can reversibly regulate the topological structure of telomere DNA by the conversion of cis-trans state under the switching of light wavelength (Wang et al., 2010) or by the supramolecular host–guest interactions under the introduction of additional substances (Tian et al., 2017). Light-triggered cleavage of molecules is also an effective way to control the structure of target sequences (O'Hagan et al., 2019; Wu et al., 2013). However, the carcinogenicity of ultraviolet light, the depth limitation of the excitation beam and complex self-assembled systems restrict the further application in cell or tissue. Additionally, the disruption of closed-loop aptamer-based structures by near-infrared stimulation is also difficult to meet the needs of *in vivo* applications due to the accompanying high temperature (Wang et al., 2015). Redox approach can avoid these drawbacks and may thus be developed.

In the study, we design a new strategy to manipulate the enzyme activity, where the redox efficacy of GSH (structure in Figure S1) is a crucial factor (Scheme 1). To obtain a high-response redox switch, O,O-bis(2′-trimethylammonium ethyl) azophenol dibromide (AzoDiTAB, structure in Figure S2) was designed and synthesized. The low-pH environment contributed by endosomes and lysosomes (Ulbrich and Subr, 2004) is beneficial to improve the efficiency of the redox switch. High-performance liquid chromatography (HPLC) and mass spectra confirmed that GSH can effectively initiate the cleavage of AzoDiTAB. In our strategy, inhibitor recognizes and inactivates enzyme, but the introduction of AzoDiTAB causes the formation of G4 structure and triggers the folding of inhibitor, which prevents contact between inhibitor and enzyme and therefor result in the recovery of enzyme activity. More importantly, GSH

treatment initiates the cleavage of AzoDiTAB and accomplishes the liberation of the inhibitor. As a result, enzyme activity is normally inhibited. Moreover, this strategy has been successfully applied to human plasma samples. Therefore, our work would open up a new route for the specific manipulation of enzyme activity within the cancer cells, and exhibit great potential in the development of future anticancer drugs.

RESULTS

Design of redox switch

In the current study, we aimed to develop a redox switch for controlling the enzyme-catalyzed systems using active substance produced inside cells. Given that increasing the electronegativity of the azobenzene molecule increases its susceptibility to reduction by GSH (Samanta et al., 2013; Lei et al., 2019), and the trimethylammonium bromide group can induce telomere DNA to G4 structure (Xing et al., 2011), compound AzoDiTAB was designed and synthesized according to published procedures as a redox molecule sensitive to GSH (Xing et al., 2011). Previous evidences indicated that the G4 can be embedded in the aptamer targeting the protein, and introducing a high-affinity molecule to trigger the conversion of DNA between a flexible state and rigid G4 under photoisomerization or supramolecular encapsulation/liberation, thereby achieving the regulation of enzyme function (Tian et al., 2016, 2017). Excitingly, GSH cleaving AzoDiTAB into aminebenzene structure may break the original interaction between human telomere DNA (h-telo sequence in Table S1) and AzoDiTAB to a large extent and thus result in the dissociation of G4. On this basis, the thrombin-fibrinogen reaction was used as the model system to demonstrate the feasibility of our strategy. For our purpose, two thrombin-binding aptamers (15Apt and 29Apt) were linked together by human telomere DNA (Itelo, sequence in Table S1) to inhibit the thrombin activity. Specially, AzoDiTAB was requested to fold Itelo into a compact structure by inducing the formation of G4 structure, due to its strong binding affinity to telomere DNA, and at the same time, the thrombin activity was switched to the "ON" state. In contrast, GSH was expected to serve as an "OFF" switch for the thrombin activity, due to its ability to initiate the cleavage of AzoDiTAB, which leads to the emergence of liberated inhibitor. Therefore, a new redox switch was designed and expected to manipulate the thrombin activity.

GSH-mediated cleavage of AzoDiTAB

The N=N double bond in the azobenzene structure is easily broken under the attack of sulfur group of GSH, resulting in the formation of aromatic amine (Figure 1A). Here, we focus on the dependence of the cleavage of AzoDiTAB molecules on the concentration of GSH in the employed range mimicking the difference between cancer and normal cells. UV-Vis spectroscopy was used as a sensitive mean to detect the response of AzoDiTAB to GSH. Figure 1B showed the marked changes in the UV-Vis signal of AzoDiTAB treated with 10 mM GSH during the continuous incubation. Obviously, a weakened signal was observed after 3 h of incubation (olive line in Figure 1B). Moreover, treatment with 50 h of incubation greatly declined the intensity of absorption band (dark yellow line in Figure 1B), suggesting the destruction of the molecular structure of AzoDiTAB. However, treatment with 0.5 mM GSH did not significantly reduce the spectral signal of the AzoDiTAB samples, even when the incubation was progressed for more than 50 h (Figure 1C), indicating the persistent presence of AzoDiTAB. For each treatment, the decrease in absorbance at 355 nm was plotted as a function of time, and the resulting curve was fitted with an exponential decay to determine the half-life (Figure S3).

Additionally, direct evidence for GSH-mediated cleavage of AzoDiTAB was provided by HPLC. Not surprisingly, 10 mM GSH treatment caused the disappearance of the absorption band of AzoDiTAB and the formation of a sharp new band (violet line in Figure 1D). Moreover, the new substance proved to be derived from the cleavage of AzoDiTAB by mass spectrometry (Figure 1E). In contrast, there was no significant difference in the HPLC signal of AzoDiTAB incubated with 0.5 mM GSH (olive line in Figure 1D), in agreement with the results of UV-Vis spectroscopy. Similar phenomenon was also observed in the color change of the incubation solution (Figure S4). It was concluded that GSH effectively initiate the cleavage of AzoDiTAB. More importantly, high concentration of GSH was more conducive to triggering this redox reaction in the employed range of concentration mimicking the difference between cells. These results illustrated that GSH has the potential to be used as a specific regulator in cancer cells or tissue.

Operation of G4 structure upon GSH-mediated cleavage of AzoDiTAB

We detected the AzoDiTAB-induced G4 formation, and assessed the ability of GSH to dissociate the G4 structure by reducing the AzoDiTAB (Figure 2A). CD spectra are a reliable and convenient tool to detect

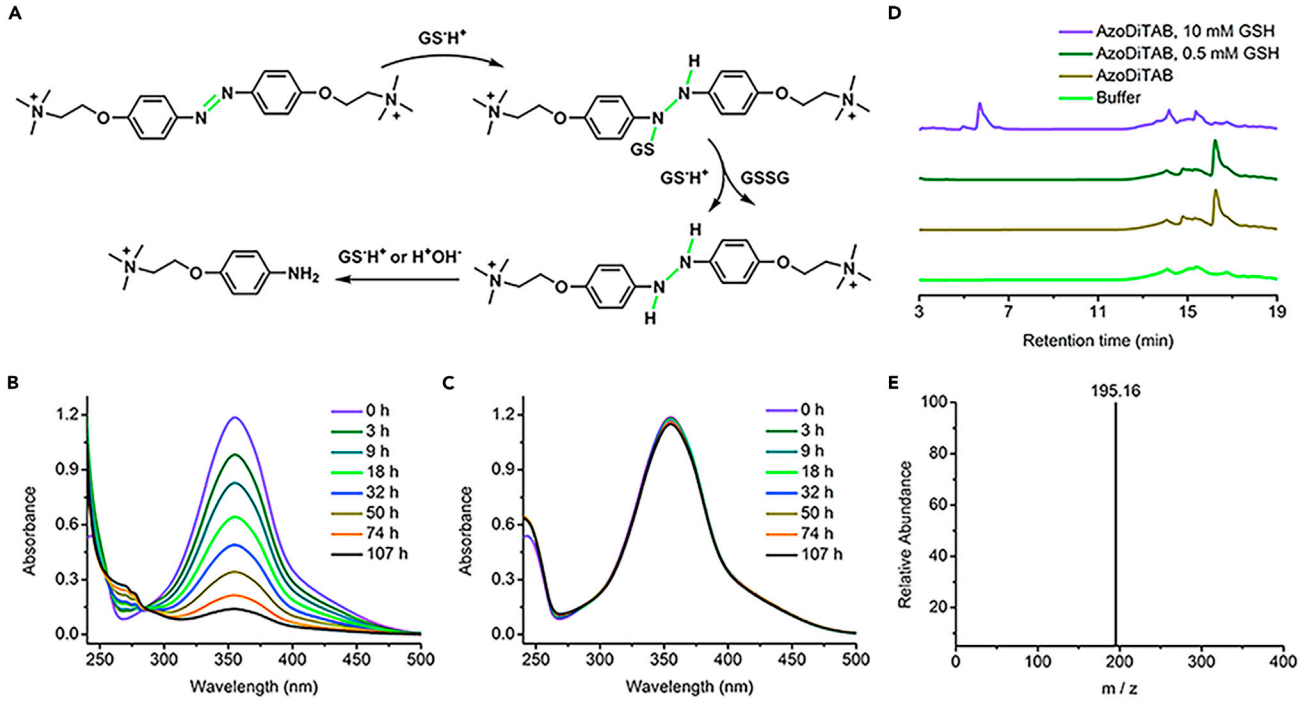

Figure 1. Characterization of the cleavage of compound AzoDTAB through GSH

(A) Schematic illustration of GSH-mediated cleavage of AzoDiTAB.

(B) Change in the absorption of AzoDiTAB (50 μM) treated with 10 mM GSH in a time range from 0 h (control) to 107 h.

(C) Change in the absorption of AzoDiTAB (50 μM) treated with 0.5 mM GSH in a time range from 0 h (control) to 107 h.

(D) HPLC of buffer (green line) and 100 μM AzoDiTAB treated with none (dark yellow line, control), 0.5 mM GSH (olive line) and 10 mM GSH (violet line).

(E) Mass spectra of new substance formed in the cleavage solution.

the second structure of DNA molecules, and we can obtain real-time information about DNA conformations from characteristic variations of CD signal. Figure 2B showed CD spectra of h-telo with AzoDiTAB treatment. Here, r was defined as [AzoDiTAB]/[h-telo]. It could be found that characteristic absorption bands of h-telo was shifted toward longer wavelength region (green line in Figure 2B) at r = 2. Evidently, peak strength was increased with increasing r value. At r = 8, h-telo presented a typical parallel-stranded G4 structure (violet line in Figure 2B) that is completely different from untreated sample, with a major positive band at approximately 265 nm and a negative band at approximately 240 nm. In addition, the thermal stability of h-telo with AzoDiTAB treatment was determined using CD at 265 nm. As r increased, thermodynamic process of h-telo changed significantly (Figure 2C), and at r = 8, a melting curve with a T_m of 45°C (blue line in Figure 2C) was observed. This behavior suggested the formation of a G4 secondary structure.

The effect of GSH-mediated cleavage of AzoDiTAB on the topological structure of h-telo was then tested. Of note, high concentration of GSH results in deviation of the CD signal in the low wavelength range (<265 nm, Figure S5). Thus, we mixed high concentration of AzoDiTAB (400 μM) and 10 mM GSH in the buffer, and the incubation solution was then diluted 5 times to corresponding AzoDiTAB concentration before the sample was tested. Strikingly, GSH treatment greatly attenuated absorption band intensity of h-telo binding to AzoDiTAB (Figure 2D). Specially, positive band at about 265 nm was significantly decreased after 15 h of incubation (blue line in Figure 2D) and this effect was more evident with increase of reaction time. More importantly, treatment with 80 h of incubation nearly entirely eliminated the contribution of AzoDiTAB to the CD signal of h-telo (olive line in Figure 2D). This finding indicated that GSH-mediated cleavage of AzoDiTAB triggered the deformation of G4 structure in a time-dependent manner. To further confirm this result, the thermal stability of these samples was determined at 265 nm. As the redox reaction progressed, the samples exhibited a large variation in absorbance over a wide range of temperature (Figure 2E). As expected, treatment with 15 h of incubation significantly reduced absorbance of h-telo (cyan line in Figure 2E). Moreover, the enhancement in CD absorption was nearly completely eliminated after 80 h of incubation (green line in Figure 2E), suggesting that the deformation of G4 structure occurred.

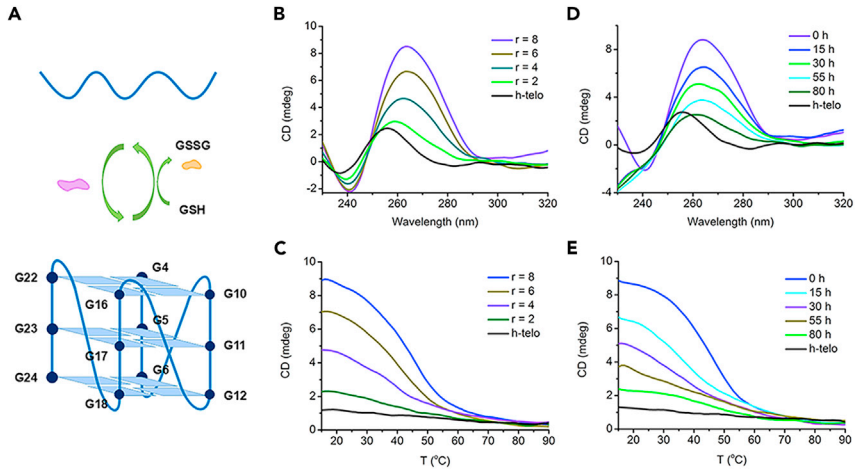

Figure 2. GSH-induced the conversion of G4 structure by cleaving AzoDiTAB

(A) Schematic illustration of the modulation of G4 structure through GSH-mediated cleavage of AzoDiTAB.

(B) CD spectra of G4 formation induced by AzoDiTAB in various concentration range from 0 μM (r = 0, control) to 80 μM (r = 8).

(C) CD melting profile of h-telo treated with various concentration of AzoDiTAB ranging from 0 μM (r = 0, control) to 80 μM (r = 8) at 265 nm.

(D) CD spectra of G4 dissociation in response to GSH-mediated cleavage of AzoDiTAB in a time range from 0 h (control) to 80 h.

(E) CD melting profile of h-telo treated with cleavage solution incubated in a time range from 0 h (control) to 80 h.

These results illustrated an interesting possibility that GSH can achieve the manipulation of G4 conformation through AzoDiTAB as a bridge.

To investigate whether GSH itself was able to affect the structure of h-telo, the h-telo sample was treated with various concentration of GSH in the absence of AzoDiTAB. We can observe that GSH treatment did not significantly change the absorbance of h-telo at 265 nm (Figure S5), even at a concentration of 10 mM. At the same time, no characteristic CD signal of parallel-stranded G4 structure appeared. Considering that GSH itself has a strong CD signal, this result can confirm that GSH hardly cause marked variation to the h-telo spectra (>265 nm). Similarly, absorbance of h-telo exhibited little variation over a wide range of temperature, as reflected in thermal melting curve (Figure S6), indicating GSH itself failed to affect topological state of h-telo. Therefore, the fact was confirmed that deformation of G4 structure was attributed to GSH-mediated cleavage of AzoDiTAB.

Controlling the thrombin activity using active molecule

Next, we employed the thrombin-fibrinogen reaction as a model system to evaluate the thrombin activity. Fluorescence spectrometer is a common and effective method for real-time monitoring of the catalytic activity of thrombin by detecting thrombin-induced fibrinogen-fibrin transformation. The light scattering intensity of fibrinogen itself was weak, but the introduction of thrombin resulted in the conversion of fibrinogen to insoluble fibrin where the scattering intensity was significantly enhanced. When inhibitor Itelo bound into thrombin, the catalytic reaction was hindered (Figure 3A). Specially, treatment with 40 nM Itelo slowed down the enhancement of scattering signal (green line in Figure 3B) to some extent, and 80 nM Itelo almost entirely terminated the formation of fibrin (blake line in Figure 3B), indicating thrombin was inactive in this condition. As mentioned above, AzoDiTAB was able to trigger folding of telomere DNA, thus various amount of AzoDiTAB were add to inhibited clotting solution. Interestingly, this behavior converted Itelo into its compact state and effectively recovered the thrombin activity (Figure 3C). Specially, treatment with 6 μM AzoDiTAB markedly enhanced the scattering intensity (olive line in Figure 3D), and thrombin was almost completely activated after the addition of 50 μM AzoDiTAB (green line in Figure 3D). In addition, effect of AzoDiTAB itself on thrombin was detected in the absence of Itelo. We found that the light scattering signals of AzoDiTAB-treated samples were similar to those of the untreated samples (Figure S7), indicating that AzoDiTAB itself cannot act on thrombin. These results are an important step toward our goal.

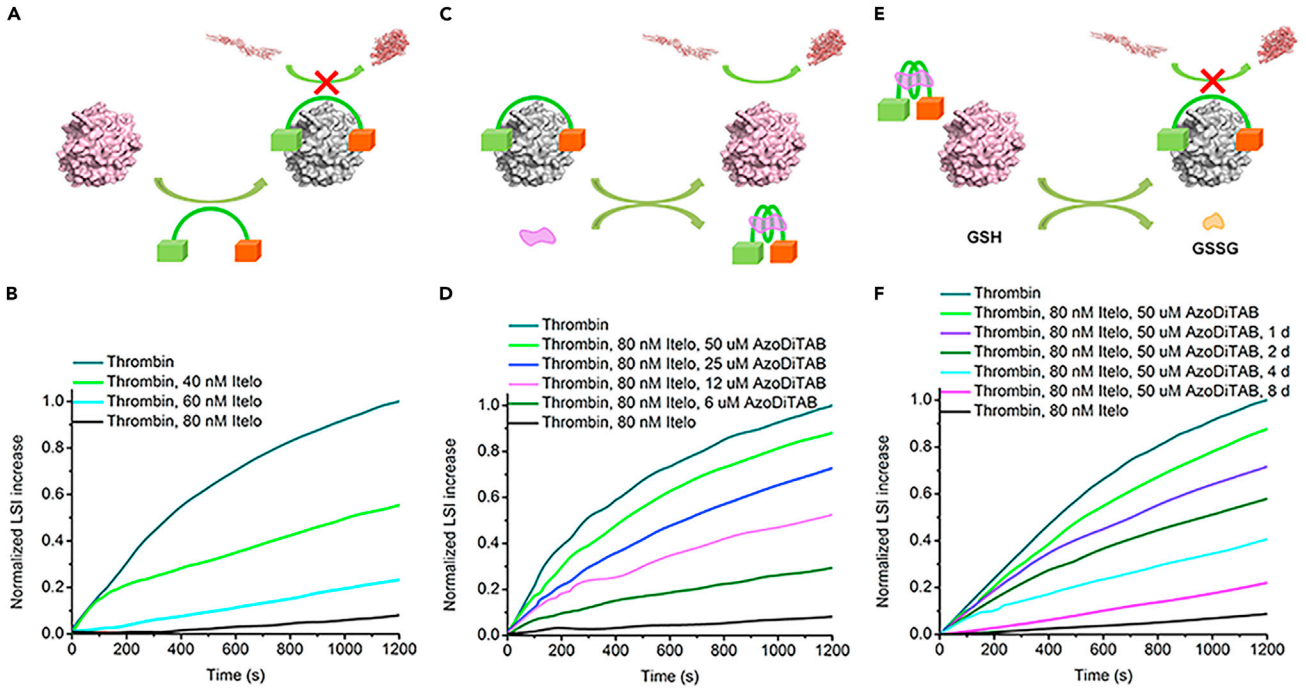

Figure 3. The transition of thrombin between active and inhibited states under different treatments

(A) Schematic representation of inactivation of thrombin by the inhibitor Itelo.

(B) Real-time light-scattering spectra of clotting reaction treated with various concentration of inhibitor Itelo ranging from 0 nM (control) to 80 nM.

(C) Schematic representation of liberation of thrombin by the compound AzoDiTAB folding inhibitor Itelo.

(D) Real-time light-scattering spectra of clotting reaction treated with inhibitor Itelo (80 nM) and various concentration of AzoDiTAB ranging from 0 μM (control) to 50 μM.

(E) Schematic representation of inhibition of thrombin by GSH-triggered cleavege of AzoDiTAB releasing inhibitor Itelo.

(F) Real-time light-scattering spectra of clotting reaction treated with inhibitor Itelo (80 nM) and the cleavage solution in a time range from 0 d (control) to 8 d.

A key step for the success of our strategy is that GSH play an excellent regulatory role in the thrombin-fibrinogen reaction, which involves GSH-induced redox reaction for rapid reductive cleavage of azobenzene. From the CD assay above, it have been known that GSH can achieve the dissociation of AzoDiTAB-induced G4 structure of telomere DNA by destroying the molecular structure of AzoDiTAB. We expected that GSH treatment was able to release free Itelo and urged thrombin to be inhibited from activity, as shown in Figure 3E. To test this process, thrombin was mixed in Itelo-treated cleavage solution. Figure 3F showed representative data for the outstanding performance of GSH in the model system. As expected, treatment of 1 day (d) of incubation decreased the light scattering intensity of sample (violet line in Figure 3F), and as reaction time increased this effect was more obvious. To our delight, treatment with 8 days of reduction nearly entirely turned thrombin into inactive state (magenta line in Figure 3F). In the experiment, for avoiding the interference of high level of GSH, high concentration of AzoDiTAB (500 μM) was incubated with 10 mM GSH, and the mixture was then diluted 10 times to corresponding AzoDiTAB concentration and low GSH level before the sample was tested. It should be mentioned that the incubation time required to reverse the thrombin activity would be greatly reduced if 50 μM AzoDiTAB was directly treated with 10 mM GSH. This treatment method was kept in subsequent experiments.

Considering the change in solution after incubation, the clotting sample was treated with various reaction time of cleavage solution in the absence of Itelo. Our result indicated that cleavage solution itself cannot significantly interfere the normal progress of clotting reaction (Figure S8), even those of longer reaction time. These findings suggested that our strategy was expected to manipulate the activity of enzyme using physiologically active molecule.

Dynamic morphology analysis of fibrin based on redox switch

Clotting reaction dynamics was further monitored *in vitro* by laser scanning confocal microscopy. Here, Alexa Flour 488-labeled fibrinogen was used as the substrate. Fibrinogen itself was stable in solution,

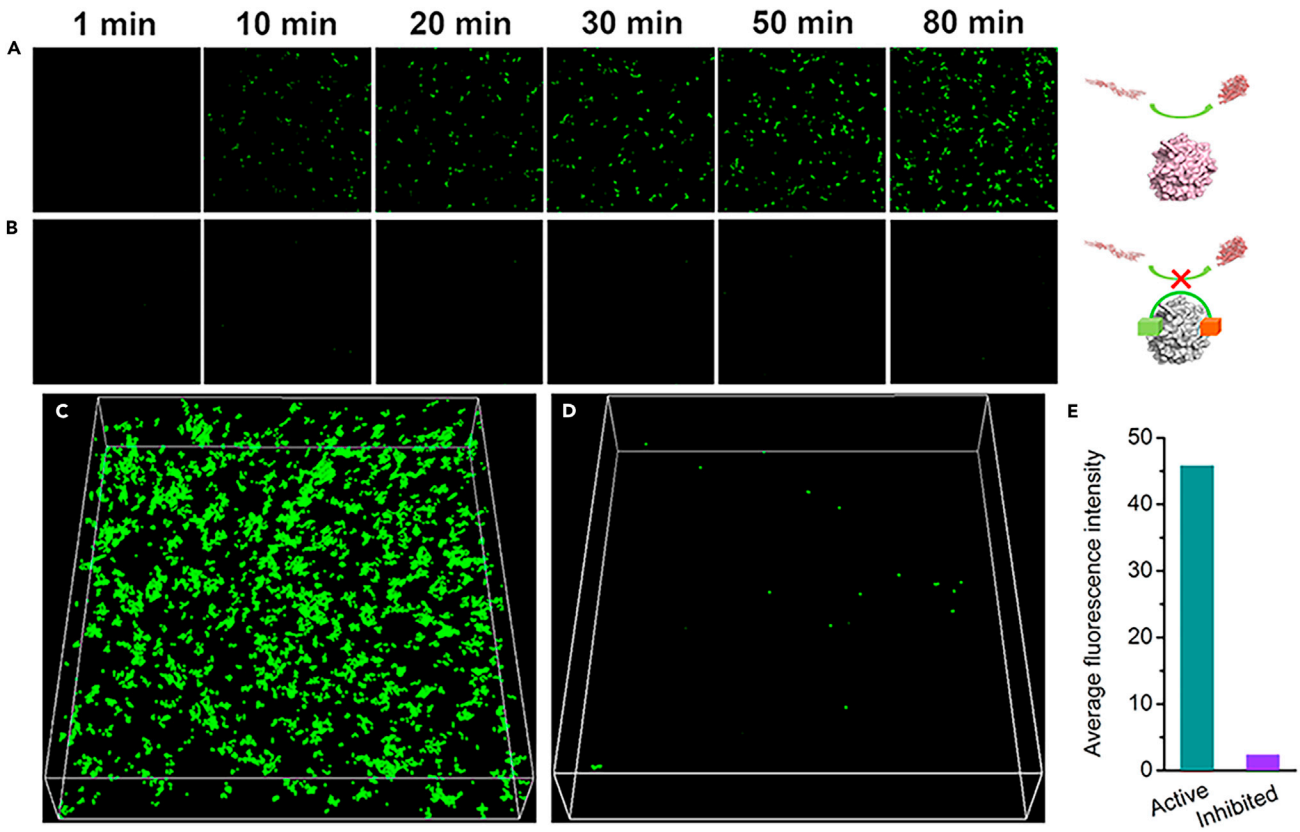

Figure 4. *In situ* detection of clotting reaction dynamics under normal and inhibited conditions

(A) Dynamic morphology changes of fibrinogen treated with thrombin.

(B) Dynamic morphology changes of fibrinogen treated with Itelo-inhibited thrombin.

(C) 3D surface projections of Z-stack images for fibrinogen treated with thrombin at t = 80 min.

(D) 3D surface projections of Z-stack images for fibrinogen treated with Itelo-inhibited thrombin at t = 80 min.

(E) Comparison of the average fluorescence intensity between Z-stack images.

even after a long time period (Figure S9). After the addition of thrombin, dynamic morphological variation of fibrinogen occurred. As shown in Figure 4A, the formation of fibrin fibers was hardly found at t = 1 min, but fibrinogen was continuously aggregated into large fibrin fibers with increasing catalytic reaction time, and this effect was more intuitive at t = 80 min. As for Itelo-treated sample, only fibrin oligomers were observed, and its dynamic morphology maintained stable throughout the catalytic process (Figure 4B), reflecting the efficient inhibition of thrombin activity. Z-stack images clearly showed the density and distribution of fibrin fibers in solution. No surprisingly, for three-dimensional images obtained at t = 80 min, the thrombin-catalyzed sample presented a high fibrin fibers density (Figure 4C) while inhibited catalyzed sample almost wholly terminated formation of large fibrin fibers (Figure 4D). The average fluorescence intensity between the Z-stack images were quantified to further reveal the inhibitory efficacy of Itelo with the image processing software (Figure 4E).

When the inhibited catalyzed sample was treated with AzoDiTAB a marked conversion of fibrinogen into fibrin could be recognized (Figure 5A), and the aggregation rate of this process resembled those of untreated sample, indicating AzoDiTAB urged thrombin to recover from inactivity. We then detected the effect of GSH on AzoDiTAB activated clotting reaction. Strikingly, after the structure of AzoDiTAB was destroyed by GSH, no typical large fibrin fibers could be noticed, even at t = 80 min (Figure 5B). We discovered the fact that GSH-mediated cleavage of AzoDiTAB released Itelo and inactivated thrombin. Three-dimensional images of AzoDiTAB activated catalyzed sample presented large quantities fibrin networks (Figure 5C), whereas the size and intensity of fiber bundles could nearly wholly be neglected for the inhibited sample treated with GSH-cleavaged AzoDiTAB (Figure 5D). Similarly, the obvious distinctions caused by different treatments were reflected in the average fluorescence intensity of Z-stack image (Figure 5E).

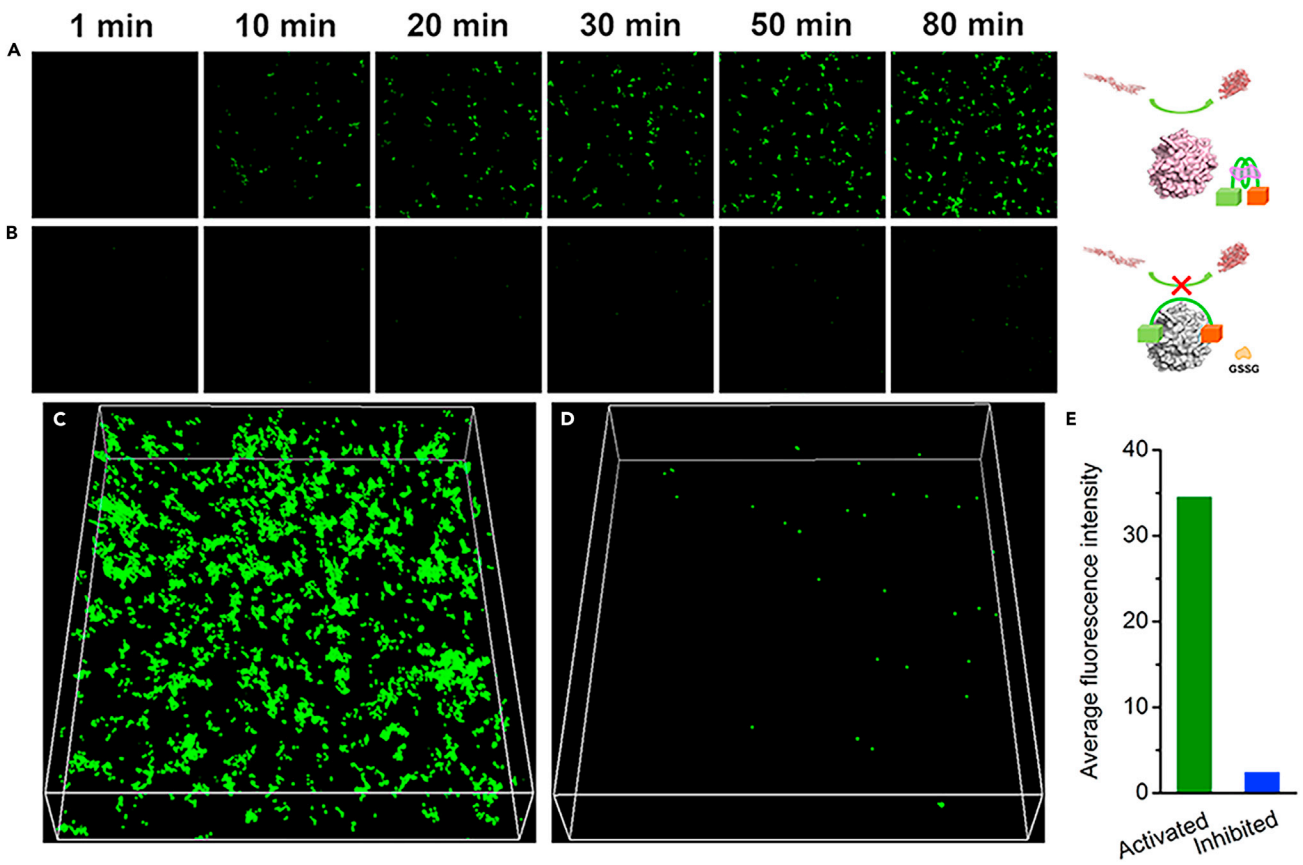

Figure 5. *In situ* detection of clotting reaction dynamics under activated and inhibited conditions

(A) Dynamic morphology changes of fibrinogen treated with activated thrombin by AzoDiTAB folding inhibitor Itelo.

(B) Dynamic morphology changes of fibrinogen treated with inhibited thrombin by GSH-triggered cleavage of AzoDiTAB releasing inhibitor Itelo.

(C) 3D surface projections of Z-stack images for fibrinogen treated with activated thrombin by AzoDiTAB folding inhibitor Itelo at t = 80 min.

(D) 3D surface projections of Z-stack images for fibrinogen treated with inhibited thrombin by GSH-triggered cleavage of AzoDiTAB releasing inhibitor Itelo at t = 80 min.

(E) Comparison of the average fluorescence intensity between Z-stack images.

Additionally, we also noticed that neither AzoDiTAB nor GSH-cleavaged AzoDiTAB could trigger the conversion of fibrinogen into fibrin without thrombin (Figure S10), and neither of them affected the normal progress of clotting reaction with thrombin (Figure S11). These findings therefore illustrated the outstanding ability of GSH to regulate the thrombin activity.

Redox regulation of the clot formation in the human plasma

Our strategy has achieved the redox regulation of enzyme activity *in vitro*, meaning it has the potential to be applied in complex biological samples. To test this mechanism, human plasma samples were used in the clotting reaction. The thrombin time (TT) assay is a reliable method to measure the time required for a clot formation in the plasma from a blood sample. As shown in Tables 1 and S2, the TT of the thrombin sample was 18.8 s. While the TT of Itelo-treated thrombin samples was 68.2 s, which was 3.6 times longer than those of untreated samples, indicating that thrombin activity is largely inhibited. As for inhibited thrombin samples treated with AzoDiTAB, a TT (23.3 s) similar to those of untreated samples was observed. This result illustrated robust recovery of thrombin activity. More importantly, there was a significant difference after AzoDiTAB was reduced by GSH. The plasma samples exhibited a TT of 66.4 s, 2.8 times longer than those of liberated thrombin samples, demonstrating the inhibition of thrombin activity and the longer clotting process. Of note, the MTT assay indicated that AzoDiTAB treatment in the employed concentration range did not significantly reduce the viability of cultured A549 cells (Figure S12). Above results absolutely confirmed that our strategy can be applied to real biological samples.

Table 1. Biological effects of redox switch

Samples	T-time (s)[a]
Control	18.8 ± 0.5
Itelo	68.2 ± 0.8
Itelo, AzoDiTAB	23.3 ± 1.5
Itelo, GSH-cleavaged AzoDiTAB	64.4 ± 0.4

[a]"T-time" is the time required for a clot formation in the plasma from a blood sample.

DISCUSSION

Our work mainly focuses on active molecules produced inside cells that can directly or indirectly participate in the control of enzyme-catalyzed systems. Degradation of AzoDiTAB via GSH-mediated reduction to the respective aminobenzene structure was confirmed through UV-Vis spectroscopy, HPLC and mass spectrometry measurements, and this redox reaction was more easily triggered by high level of GSH in the range of concentration used to mimic the difference between cancer and normal cells, which exhibits great promise for targeting cancel cells since GSH is present in cancer cells at concentrations up to 10 mM (Raderer and Scheithauer, 1993; Perry et al., 1993; Berger et al., 1994; Redmond et al., 1991; Oberlischrammli et al., 1994; Cook et al., 1991; Joncourt et al., 1995; Mulder et al., 1995). Unlike hydrazobenzenes formed in the incomplete reduction of azobenzene molecules through GSH in most cases (Boulegue et al., 2007; Samanta et al., 2013; Kosower and Kanetylondner, 1976), high toxicity was shown in carcinogenic aromatic amines stemmed from the GSH-mediated cleavage of AzoDiTAB which upon oxidation form species that bind to DNA covalently (Brown and De Vito, 1993). This feature has the potential to induce cancer cells apoptosis. Our results revealed that half of AzoDiTAB (50μM) was bleached after 21 h of treatment ($t_{1/2}$ = 21 h at 10 mM GSH) and substrate almost completely disappeared with increasing incubation time, which was attributed to high electronegativity of AzoDiTAB that increases the susceptibility to reduction by GSH (Samanta et al., 2013; Lei et al., 2019). It was subsequently confirmed that GSH cleaving AzoDiTAB resulted in the transition of telomere DNA structures between the rigid G4 and a flexible state by breaking the interaction between DNA and AzoDiTAB. Importantly, this redox-based method for the modulation of G4 can avoid the defects of external stimulus such as light (Wang et al., 2010; O'Hagan et al., 2019) and temperature (Wang et al., 2015) *in vivo* application.

Based on the above results, we achieved the conversion of thrombin from being free to be inhibited through GSH-mediated cleavage of AzoDiTAB in the presence of inhibitor Itelo. The human plasma assay further demonstrated the possibility of application in organisms. In fact, the incubation time required to trigger the inactivation of thrombin in the experiment will be greatly reduced according to the results of UV-Vis spectra if 10 mM GSH was directly employed in model system. Compared with previous strategies, the redox switch described here can be specifically applied to the modulation of enzyme-catalyzed system in cancer cells without external stimulus due to the varying amounts of GSH in different cells and even can induce cancer cells apoptosis due to the formation of carcinogenic aromatic amines. This strategy will be beneficial to antitumor exploration and pharmaceutical development.

Limitations of the study

In this work, high concentration of AzoDiTAB was added to induce the formation of G4, which triggers the folding of inhibitor Itelo and causes the recovery of thrombin activity. Under harsh physiological conditions, the need to elevated the concentration of small molecule ligands may result in a decrease in regulation efficiency. Therefore, it is still necessary to develop a ligand with higher binding affinity for G4 DNA. In addition, future work is needed to evaluate the applicability of the developed redox switch in vivo and the efficiency of targeting cancer cells.

STAR★METHODS

Detailed methods are provided in the online version of this paper and include the following:

- KEY RESOURCES TABLE
- RESOURCE AVAILABILITY
  - Lead contact
  - Materials availability
  - Data and code availability
- EXPERIMENTAL MODELS AND SUBJECT DETAILS

SUPPLEMENTAL INFORMATION

Supplemental information can be found online at https://doi.org/10.1016/j.isci.2021.102977.

ACKNOWLEDGMENTS

The authors are grateful to Prof Zhenjun Yang for equipment support. This work was supported by National Natural Science Foundation of China (grant number 21778054, 51772289, 51972302), Beijing Natural Science Foundation (grant number 2192058), National Key Research and Development Program of China (grant number 2016YFF0203700), State Key Laboratory of Natural and Biomimetic Drugs (grant number K20180202), Fundamental Research Funds for the Central Universities.

AUTHOR CONTRIBUTIONS

Conceptualization, D.L., X.L., Y.H., and L.W., Methodology, X.T., X.L., Y.H., and L.W., Investigation, D.L.,Y.K., L.Y., Y.K., Y.Z., and H.L., Original Draft, D.L., Supervision and Funding Acquisition, X.L., Y.H., and L.W.

DECLARATION OF INTERESTS

The authors declare no competing interests.

Received: January 27, 2021
Revised: July 1, 2021
Accepted: August 9, 2021
Published: September 24, 2021

REFERENCES

Anderson, M.E. (1998). Glutathione: an overview of biosynthesis and modulation. Chem. Biol. Interact. *112*, 1–14.

Bauri, K., Nandi, M., and De, P. (2018). Amino acid-derived stimuli-responsive polymers and their applications. Polym. Chem. *9*, 1257–1287.

Berger, S.J., Gosky, D., Zborowska, E., Willson, J.K.V., and Berger, N.A. (1994). Sensitive enzymatic cycling assay for glutathione: measurements of glutathione content and its modulation by buthionine sulfoximine in vivo and in vitro in human colon cancer. Cancer Res. *54*, 4077–4083.

Biffi, G., Tannahill, D., McCafferty, J., and Balasubramanian, S. (2013). Quantitative visualization of DNA G-quadruplex structures in human cells. Nat. Chem. *5*, 182–186.

Boulegue, C., Loweneck, M., Renner, C., and Moroder, L. (2007). Redox potential of azobenzene as an amino acid residue in peptides. Chembiochem *8*, 591–594.

Brown, M.A., and De Vito, S.C. (1993). Predicting azo dye toxicity. Crit. Rev. Environ. Sci. Technol. *23*, 249–324.

Cook, J.A., Pass, H.I., Iype, S.N., Friedman, N., Degraff, W., Russo, A., and Mitchell, J.B. (1991). Cellular glutathione and thiol measurements from surgically resected human lung tumor and normal lung tissue. Cancer Res. *51*, 4287–4294.

Eom, T., Yoo, W., Kim, S., and Khan, A. (2018). Biologically activatable azobenzene polymers targeted at drug delivery and imaging applications. Biomaterials *185*, 333–347.

Fuhrmann, J., Subramanian, V., and Thompson, P.R. (2013). Targeting the arginine phosphatase YwlE with a catalytic redox-based inhibitor. ACS Chem. Biol. *8*, 2024–2032.

Guglielmi, G., Falk, H.J., and De Renzis, S. (2016). Optogenetic control of protein function: from intracellular processes to tissue morphogenesis. Trends Cell Biol. *26*, 864–874.

Haydell, M.W., Centola, M., Adam, V., Valero, J., and Famulok, M. (2018). Temporal and reversible control of a DNAzyme by orthogonal photoswitching. J. Am. Chem. Soc. *140*, 16868–16872.

Hull, K., Morstein, J., and Trauner, D. (2018). In vivo photopharmacology. Chem. Rev. *118*, 10710–10747.

Hwang, C., Sinskey, A.J., and Lodish, H.F. (1992). Oxidized redox state of glutathione in the endoplasmic reticulum. Science *257*, 1496–1502.

Joncourt, F., Oberli-Schrammli, A.E., Stadler, M., Buser, K., Franscini, L., Fey, M.F., and Cerny, T.

(1995). Patterns of drug resistance parameters in adult leukemia. Leuk. Lymphoma *17*, 101–109.

Kim, Y., Phillips, J.A., Liu, H., Kang, H., and Tan, W. (2009). Using photons to manipulate enzyme inhibition by an azobenzene-modified nucleic acid probe. Proc. Natl. Acad. Sci. U S A *106*, 6489–6494.

Kim, S.H., Kim, K.R., Ahn, D.R., Lee, J.E., Yang, E.G., and Kim, S.Y. (2017). Reversible regulation of enzyme activity by pH-responsive encapsulation in DNA nanocages. ACS Nano *11*, 9352–9359.

Kosower, E.M., and Kanetylondner, H. (1976). Glutathione. 13. mechanism of thiol oxidation by diazenedicarboxylic acid derivatives. J. Am. Chem. Soc. *98*, 3001–3007.

Kosower, N.S., and Kosower, E.M. (1978). The glutathione status of cells. Int. Rev. Cytol. *54*, 109–160.

Kovacic, M., Podbevsek, P., Tateishi-Karimata, H., Takahashi, S., Sugimoto, N., and Plavec, J. (2020). Thrombin binding aptamer G-quadruplex stabilized by pyrene-modified nucleotides. Nucleic Acids Res. *48*, 3975–3986.

Lee, M.H., Yang, Z., Lim, C.W., Lee, Y.H., Dongbang, S., Kang, C., and Kim, J.S. (2013). Disulfide-cleavage-triggered chemosensors and their biological applications. Chem. Rev. *113*, 5071–5109.

Lee, S.H., Moroz, E., Castagner, B., and Leroux, J.C. (2014). Activatable cell penetrating peptide-peptide nucleic acid conjugate via reduction of azobenzene PEG chains. J. Am. Chem. Soc. *136*, 12868–12871.

Lei, H., Mo, M., He, Y., Wu, Y., Zhu, W., and Wu, L. (2019). Bioactivatable reductive cleavage of azobenzene for controlling functional dumbbell oligodeoxynucleotides. Bioorg. Chem. *91*, 103106.

Lubbe, A.S., Szymanski, W., and Feringa, B.L. (2017). Recent developments in reversible photoregulation of oligonucleotide structure and function. Chem. Soc. Rev. *46*, 1052–1079.

Medina, S.H., Chevliakov, M.V., Tiruchinapally, G., Durmaz, Y.Y., Kuruvilla, S.P., and Elsayed, M.E. (2013). Enzyme-activated nanoconjugates for tunable release of doxorubicin in hepatic cancer cells. Biomaterials *34*, 4655–4666.

Meister, A. (1994). Glutathione, ascorbate, and cellular protection. Cancer Res. *54*, 1969S–1975S.

Mergny, J.L., and Sen, D. (2019). DNA quadruple helices in nanotechnology. Chem. Rev. *119*, 6290–6325.

Mo, M., Kong, D., Ji, H., Lin, D., Tang, X., Yang, Z., He, Y., and Wu, L. (2019). Reversible photocontrol of thrombin activity by replacing loops of thrombin binding aptamer using azobenzene derivatives. Bioconjug. Chem *30*, 231–241.

Mulder, T.P.J., Manni, J.J., Roelofs, H.M.J., Peters, W.H.M., and Wiersma, A. (1995). Glutathione S-transferases and glutathione in human head and neck cancer. Carcinogenesis *16*, 619–624.

O'Hagan, M.P., Haldar, S., Duchi, M., Oliver, T.A.A., Mulholland, A.J., Morales, J.C., and Galan, M.C. (2019). A photoresponsive stiff-stilbene ligand fuels the reversible unfolding of G-quadruplex DNA. Angew. Chem. Int. Ed. *58*, 4334–4338.

Oberlischrammli, A.E., Joncourt, F., Stadler, M., Altermatt, H.J., Buser, K., Ris, H.B., Schmid, U., and Cerny, T. (1994). Parallel assessment of glutathione-based detoxifying enzymes, O6-alkylguanine-DNA alkyltransferase and P-glycoprotein as indicators of drug resistance in tumor and normal lung of patients with lung cancer. Int. J. Cancer *59*, 629–636.

Panigaj, M., Johnson, M.B., Ke, W., McMillan, J., Goncharova, E.A., Chandler, M., and Afonin, K.A. (2019). Aptamers as modular components of therapeutic nucleic acid nanotechnology. ACS Nano *13*, 12301–12321.

Pasternak, A., Hernandez, F.J., Rasmussen, L.M., Vester, B., and Wengel, J. (2011). Improved thrombin binding aptamer by incorporation of a single unlocked nucleic acid monomer. Nucleic Acids Res. *39*, 1155–1164.

Perry, R.R., Mazetta, J., Levin, M., and Barranco, S.C. (1993). Glutathione levels and variability in breast tumors and normal tissue. Cancer *72*, 783–787.

Raderer, M., and Scheithauer, W. (1993). Clinical trials of agents that reverse multidrug resistance. A. Literature Review. Cancer *72*, 3553–3563.

Rane, C.K., and Minden, A. (2019). P21 activated kinase signaling in cancer. Semin. Cancer Biol. *54*, 40–49.

Redmond, S.M.S., Joncourt, F., Buser, K., Ziemiecki, A., Altermatt, H.J., Fey, M., Margison, G., and Cerny, T. (1991). Assessment of p-glycoprotein glutathione-based detoxifying enzymes and O6-alkylguanine-DNA alkyltransferase as protein indicators of constitutive drug-resistance in human colorectal tumors. Cancer Res. *51*, 2092–2097.

Saito, G., Swanson, J.A., and Lee, K.D. (2003). Drug delivery strategy utilizing conjugation via reversible disulfide linkages: role and site of cellular reducing activities. Adv. Drug Deliv. Rev. *55*, 199–215.

Samanta, S., Beharry, A.A., Sadovski, O., McCormick, T.M., Babalhavaeji, A., Tropepe, V., and Woolley, G.A. (2013). Photoswitching azo compounds in vivo with red light. J. Am. Chem. Soc. *135*, 9777–9784.

Tian, T., Song, Y., Wang, J., Fu, B., He, Z., Xu, X., Li, A., Zhou, X., Wang, S., and Zhou, X. (2016). Small-molecule-triggered and light-controlled reversible regulation of enzymatic activity. J. Am. Chem. Soc. *138*, 955–961.

Tian, T., Song, Y., Wei, L., Wang, J., Fu, B., He, Z., Yang, X.R., Wu, F., Xu, G., Liu, S.M., et al. (2017). Reversible manipulation of the G-quadruplex structures and enzymatic reactions through supramolecular host-guest interactions. Nucleic Acids Res. *45*, 2283–2293.

Tischer, D., and Weiner, O.D. (2014). Illuminating cell signalling with optogenetic tools. Nat. Rev. Mol. Cell Biol. *15*, 551–558.

Trachootham, D., Alexandre, J., and Huang, P. (2009). Targeting cancer cells by ROS-mediated mechanisms: a radical therapeutic approach? Nat. Rev. Drug Discov. *8*, 579–591.

Ulbrich, K., and Subr, V. (2004). Polymeric anticancer drugs with pH-controlled activation. Adv. Drug Deliv. Rev. *56*, 1023–1050.

Virgilio, A., Petraccone, L., Vellecco, V., Bucci, M., Varra, M., Irace, C., Santamaria, R., Pepe, A., Mayol, L., Esposito, V., et al. (2015). Site-specific replacement of the thymine methyl group by fluorine in thrombin binding aptamer significantly improves structural stability and anticoagulant activity. Nucleic Acids Res. *43*, 10602–10611.

Wang, X., Huang, J., Zhou, Y., Yan, S., Weng, X., Wu, X., Deng, M., and Zhou, X. (2010). Conformational switching of G-quadruplex DNA by photoregulation. Angew. Chem. Int. Ed. *49*, 5305–5309.

Wang, F., Travins, J., DeLaBarre, B., Penard-Lacronique, V., Schalm, S., Hansen, E., Straley, K., Kernytsky, A., Liu, W., Gliser, C., et al. (2013). Targeted inhibition of mutant IDH2 in leukemia cells induces cellular differentiation. Science *340*, 622–626.

Wang, J., Wei, Y., Hu, X., Fang, Y.Y., Li, X., Liu, J., Wang, S., and Yuan, Q. (2015). Protein activity regulation: inhibition by closed-loop aptamer-based structures and restoration by near-IR stimulation. J. Am. Chem. Soc. *137*, 10576–10584.

Wu, L., Wang, Y., Wu, J., Lv, C., Wang, J., and Tang, X. (2013). Caged circular antisense oligonucleotides for photomodulation of RNA digestion and gene expression in cells. Nucleic Acids Res. *41*, 677–686.

Wu, J., Kumar, S., Wang, F., Wang, H., Chen, L., Arsenault, P., Mattern, M., and Weinstock, J. (2018). Chemical approaches to intervening in ubiquitin specific protease 7 (USP7) function for oncology and immune oncology therapies. J. Med. Chem. *61*, 422–443.

Xing, X., Wang, X., Xu, L., Tai, Y., Dai, L., Zheng, X., Mao, W., Xu, X., and Zhou, X. (2011). Light-driven conformational regulation of human telomeric G-quadruplex DNA in physiological conditions. Org. Biomol. Chem. *9*, 6639–6645.

Zhang, K., and Cui, B. (2015). Optogenetic control of intracellular signaling pathways. Trends Biotechnol. *33*, 92–100.

Zhang, L., Wang, Y., Zhang, X., Wei, X., Xiong, X., and Zhou, S. (2017). Enzyme and redox dual-triggered intracellular release from actively targeted polymeric micelles. ACS Appl. Mater. Interfaces *9*, 3388–3399.

STAR★METHODS

KEY RESOURCES TABLE

REAGENT or RESOURCE	SOURCE	IDENTIFIER
Chemicals, Peptides, and Recombinant proteins		
Glutathione	3A	CAS# 70-18-8
Sodium hydroxide	3A	CAS# 1310-73-2
Potassium carbonate	3A	CAS# 584-08-7
Tris base	Sigma-Aldrich	CAS# 77-86-1
Hydrochloric acid	Sigma-Aldrich	CAS# 7647-01-0
Potassium chloride	Sigma-Aldrich	CAS# 7447-40-7
Fibrinogen from human plasma	Sigma-Aldrich	F3879
Alexa Fluor 488-labeled fibrinogen	Sigma-Aldrich	F13191
4-Aminophenol	Innochem	CAS# 123-30-8
Phenol	Innochem	CAS# 108-95-2
1,2-dibromoethane	Innochem	CAS# 106-93-4
Trimethylamine (33 wt.%) solution in ethanol	Lushi	CAS# 75-50-3
Ethanol absolute	aladdin	CAS# 64-17-5
Methanol	aladdin	CAS# 67-56-1
Ethyl ether	Wokai	CAS# 60-29-7
Sodium nitrite	Macklin	CAS# 7632-00-0
Oligonucleotides		
h-telo	Sangon Biotech	N/A
Itelo	Sangon Biotech	N/A

RESOURCE AVAILABILITY

Lead contact

All requests for additional information and reagents should be directed to the Lead Contact, Li Wu (wuli@ucas.ac.cn).

Materials availability

This study did not generate new unique reagents.

Data and code availability

All data reported in this paper will be shared by the lead contact upon request. This study did not generate any data sets or code. Any additional information required to reanalyze the data reported in this paper is available from the lead contact upon request.

EXPERIMENTAL MODELS AND SUBJECT DETAILS

Blood from healthy individuals was added to a tube containing 109 mM sodium citrate. The mixture was subsequently centrifuged for 5 min at 3000 rpm at room temperature to remove blood cells, and resulting plasma was used for measurement.

METHOD DETAILS

Synthesis and cleavage

Compound AzoDiTAB was synthesized according to the previous literature (Xing et al., 2011). The cleavage of AzoDiTAB followed the steps below. To 10 mM GSH solution in 10 mM Tris-HCl buffer (pH 4.8) AzoDiTAB

was added to reach final concentration. The mixture was subsequently incubated at 37°C in a 200 rpm shaker.

4,4′-(1,2-diazenediyl)bisphenol (AzoDiOH)

p-Aminophenol (45.87 mmol, 1 .00 equiv) was dissolved in diluted aqueous HCl (1 M, 100.00 mL) and cooled to 0°C. An aqueous solution of NaNO2 (68.81 mmol, 1.50 equiv) and methanol (100.00 mL) were added dropwise in this order. Subsequently, a prepared suspension of phenol (50.42 mmol, 1.10 equiv) and NaOH (100.00 mmol, 2.00 equiv) in cold water (33.00 mL) was added slowly, and the reaction mixture was stirred for 2 h at room temperature. After adjusting the pH to 3 with concentrated HCl, the solution was extracted with diethyl ether, dried over Na2SO4 and concentrated to dryness. Finally, the crude product was purified by silica gel column chromatography (chloroform) to obtain a brown solid (4.4 g, 45% yield). ^{1}H-NMR (400 MHz, DMSO-d6), 1 .00 equiv) was dissolved in diluted aqueous HCl (1 M, 100.00 mL) a^{13}C-NMR (101 MHz, DMSO-d6):, 1 .00 equiv) was dissolved in diluted aqueous HCl (1 M, 100.00 mL) an^{+})$^{+}$: 215.0815, found: 215.0807.

1,2-bis[4-(2-bromoethoxy)phenyl]diazene (AzoDiBr)

To a solution of 1, 2-dibromoethane (28.02 mmol, 6.00 equiv) in dry acetone (46.00 mL) were added slowly AzoDiOH (4.67 mmol,1.00 equiv) and anhydrous K2CO3 (32.69 mmol, 7.00 equiv) in this order. The reaction mixture was stirred under reflux for 48 h, then hot filter and washed several times with excess hot acetone, combined filtrate was concentrated to dryness in vacuo. The yellow solid (1.02 g, 51% yield) was obtained from recrystallization (acetone/water = 1/3). ^{1}H-NMR (400 MHz, CDCl3):ibromoethane (28.02 mmol, 6.00 equiv) in dry acetone (46.00 mL) were added slowly AzoDiOH (4.^{13}C-NMR (101 MHz, CDCl3):ibromoethane (28.02 mmol, 6.00 equiv) in dry acetone (46.00 mL) were added slowly AzoDiO^{+})$^{+}$: 426.9651, found: 426.9648.

O,O-bis(2′-trimethylammoniumethyl)azophenol dibromide (AzoDiTAB)

AzoDiBr (1.15mmol, 1.00 equiv) was added to trimethylamine (100.00 mL 33% ethanol solution) under Ar atmosphere, and the reaction mixture was stirred under reflux for 12 h. Subsequently, excess trimethylamine and ethanol were removed in vacuo, and the residue was recrystallized from methanol/diethyl ether (1:5) to a yellow solid (0.28 g, 62.0% yield). ^{1}H-NMR (400 MHz, DMSO-d6): δ = 3.23 (s, 18H), 3.86 (t, J = 4.7 Hz, 4H), 4.59 (t, J = 4.5 Hz, 4H), 7.17–7.23 (m, 4H), 7.87–7.92 (m, 4H). ^{13}C-NMR (101 MHz, DMSO-d6): δ = 53.22, 62.16, 64.11, 115.47, 124.30, 159.77. HRMS-ESI for C22H34Br2N4O2: calcd. ([M-2Br]/2)$^{+}$: 193.1335, found: 193.1329. (M-Br-)$^{+}$: 465.1860, found: 465.1841.

UV-Vis spectroscopy studies

Measurements for GSH-mediated Cleavage of AzoDiTAB were performed on a Shimadzu UV-2550 UV-Vis spectrophotometer using trace quartz cuvettes (d = 10 mm). The spectra signals were recorded in the 240–500 nm wavelength range at a middle speed. 50 μM AzoDiTAB was incubated with 10 mM or 0.5 mM GSH, and the incubation samples were detected in a time range from 0 h (control) to 107 h. Before the measurement, the signal of the buffer was subtracted from the spectra of the samples.

High-performance liquid chromatography (HPLC) measurement

GSH-mediated cleavage of AzoDiTAB measurement was perform on a high-performance liquid chromatography (Angilent 1260, ZORBAX Eclipse XDB C18, 5 μm, 9.4 × 250 mm) with a appropriate gradient (A: 0.05 M TEAA; B: CH3CN, 0–5 min: 95% A; 5% B, 10 min: 80% A; 20% B, 17–20 min: 0% A; 100% B), and the molecular weight of new substance was measured on a HPLC-ESI-IT-MS equipped with a diode-array detector (Ultimate 3000 UHPLC system, ThermoFisher, San Jose, CA, USA). The HPLC signals were measured at 37°C with a wavelength of 300 nm. 100 μM of AzoDiTAB was incubated with 10 mM or 0.5 mM GSH in the buffer (10 mM Tris-HCl) for 96 h.

Circular dichroism measurement

Circular dichroism (CD) spectra were recorded on a Jasco J815 Spectrometer (Japan) using 0.5 mL quartz cuvettes with a 1 mm path length at room temperature. The measurement was done in the 240–320 nm wavelength range at a scanning speed of 200 nm/min. All CD spectra were recorded three times and averaged. The melting curve at 265 nm was detected between 15 and 90°C at a scanning speed of 2°C/min. For the cleavage assay, 400 μM of AzoDiTAB was incubated with 10 mM GSH. The mixture was then diluted 5

times at a suitable time, which was used for subsequent measurement. All test samples were prepared in the buffer (10 mM Tris-HCl, pH 7.0). Before the measurement, the CD spectrum of the buffer was subtracted from the spectra of the samples.

Preparation of samples for the clotting reaction

Human thrombin was mixed in the buffer (10 mM Tris-HCl at pH 7.0, 40 mM KCl, 1mM GSH) followed by the addition of Itelo, Itelo-AzoDiTAB, or Itelo-AzoDiTAB-GSH, and the solution was equilibrated at room temperature for 15 min. For the cleavage assay, 500 μM AzoDiTAB was incubated with 10 mM GSH. The mixture was then diluted 10 times at a suitable time, and the final concentration of GSH in the test solution was maintained at 1 mM. Followed by the addition of Itelo and thrombin, and the solution was equilibrated at room temperature for 15 min. Fibrinogen was add at reaction time (t) = 0.

Real-time monitoring of catalytic activity of thrombin

This assay aimed at monitor the catalytic activity of thrombin toward the clotting reaction using the Fluorom ax-4 fluorescence spectrometer with the kinetics mode at room temperature. The light scattering intensity was measured with a 1 cm path length cell. Fibrinogen level was maintained at 0.3 mg/mL. The excitation and emission wavelengths ware both set to 650 nm. Slit width: excitation = 10 nm; emission = 7 nm. Thrombin solution without any treatment was always tested together with other samples as internal standard. All of samples were normalized based on the internal standard.

Detection of aggregation of fibrinogen

The conversion of Fibrinogen into large fibrin fibers was monitored using a laser scanning confocal microscope (Nikon A1, Japan) with an excitation wavelength at 488 nm. Fibrinogen labeled with Alexa Fluor 488 was used in this assay and was maintained at a concentration of 0.2 mg/mL. 30 uL of each sample was quickly added to the bottom of small Petri dishes, and then the coverslip was carefully placed on the liquid drop. All of the images were collected using a 20× dry objective until the clotting reaction was nearly complete. Z-stack images of samples were obtained at 80 min.

Thrombin time assay of human plasma

The regulation effect of active GSH on clotting time was determined by a thrombin time assay. Samples were prepared as described above for the clotting measurement. The TTs of Thrombin, inhibited thrombin, AzoDiTAB activated thrombin or GSH-induced inhibited thrombin solutions were detected on a Pun-2048b Two Channel Blood Coagulation Analyzer (Beijing Poulenc Medical Science and Technology Co., Ltd., China). For this assay, blood from healthy individuals was added to a tube containing 109 mM sodium citrate. The mixture was subsequently centrifuged for 5 min at 3,000 rpm at room temperature to remove blood cells, and resulting plasma was used for measurement.

Cell survival assay

Human lung carcinoma cell line A549 was grown in DMEM medium containing 10% Fetal Bovine Serum (FBS) and 1% Pen Strep at 37°C, 5% CO2 humidified atmosphere. Cells were seeded in 96-well plates (1.5×10^5 cells/mL) and incubated overnight. Cells were exposed to various concentration of AzoDiTAB for 48 h. Then, 10 ul of 5 mg/mL methylthiazolyl tetrazolium (MTT) solution was added to each well, and the cells were further incubated for 4 h. After the medium was removed, DMSO (100 uL) was added to each well and the OD values at 570 nm were detected by a microplate reader (Tecan Spark) to evaluate cell viability.

QUANTIFICATION AND STATISTICAL ANALYSIS

The statistical details of experiments can be found in Method details and in the figure legends where applicable. OriginPro 86 software was used for statistical analysis.